



Contents lists available at ScienceDirect

Inorganica Chimica Acta

journal homepage: [www.elsevier.com/locate/ica](http://www.elsevier.com/locate/ica)

Research paper

## Synthesis, reactivities and anti-cancer properties of ruthenium(II) complexes with a thiaether macrocyclic ligand<sup>☆</sup>

Hannah A. O'Riley, Aviva Levina, Jade B. Aitken, Peter A. Lay<sup>\*</sup>

School of Chemistry, The University of Sydney, Sydney, NSW 2006, Australia

## ARTICLE INFO

## Article history:

Received 23 January 2016

Received in revised form 27 July 2016

Accepted 28 July 2016

Available online xxxxx

## Keywords:

Ruthenium(II)

Thiaether

Halido

Substitution reactions

Anti-cancer properties

Invasion assays

## ABSTRACT

Drug resistance and severe patient side-effects of Pt drugs have spurred research into other metal-based pharmaceuticals and recently Ru complexes have been identified as promising anti-cancer drugs. A series of Ru<sup>II</sup> complexes [RuX<sub>2</sub>([9]aneS<sub>3</sub>)(S-dmso)] (X = Cl, Br, I, S-dmso = sulfur-bound dimethylsulfoxide) containing the neutral face-capping sulfur macrocycle ligand, 1,4,7-trithiacyclononane ([9]aneS<sub>3</sub>) was synthesized, characterized and their substitution reactions and biological activities were investigated. While the iodido complex was not sufficiently soluble for detailed studies, [RuCl<sub>2</sub>([9]aneS<sub>3</sub>)(S-dmso)] and [RuBr<sub>2</sub>([9]aneS<sub>3</sub>)(S-dmso)] were investigated to determine whether there was a direct relationship between the rates of halido ligand substitution (determined by UV/vis spectroscopy and X-ray absorption spectroscopy) and anti-cancer activities. A two-stage halido substitution process occurred in HEPES buffer (pH 7.4, 310 K). The rate constants for chlorido substitution were a factor of two larger than for the bromido analogue ((4.5 ± 0.2) × 10<sup>-4</sup> and (1.5 ± 0.1) × 10<sup>-4</sup> s<sup>-1</sup> for the chlorido complex and (2.6 ± 0.2) × 10<sup>-4</sup> and (9.2 ± 0.1) × 10<sup>-5</sup> s<sup>-1</sup> for the bromido complex). The corresponding rate constants were a factor of two to three times larger in cell culture media, but the same trends were observed. There was also a third slower reaction in media that had the same rate constant irrespective of the starting complex ((3.6 ± 0.7) × 10<sup>-5</sup> and (3.9 ± 0.3) × 10<sup>-5</sup> s<sup>-1</sup>, respectively). Neither complex exhibited significant cytotoxicity. However, both complexes exhibited anti-invasive properties to highly invasive MDA-MB-231 breast cancer cells. The more reactive chlorido complex was also the most active in the invasion assay when either the cells were treated prior to the addition to collagen matrix, or the top collagen matrix was treated with Ru after adding it to cover the cells and wound.

© 2016 Elsevier B.V. All rights reserved.

## 1. Introduction

While advances in chemotherapy, radiotherapy and surgical practices for the treatment of primary tumors have improved cures and treatments, particularly for early stage cancers [1], cancer is still a major cause of mortality. Most deaths occur in advanced cancers due to metastatic spread, either apparent or not detected [1,2]. Hence, metastasis is the cause of over 90% of cancer related deaths [2], and the probability of a cure for a cancer falls substantially once metastasis has occurred [2,3]. The development of chemopreventive treatments for metastases and the treatments of metastases has, therefore, the potential to significantly lower cancer mortality rates, increase patient longevity, and improve symptoms in those not cured.

Research into Ru anti-metastatic and cytotoxic drugs has been gaining momentum [4–12], following the success of imidazolium *trans*-tetrachlorido(*S*-dimethylsulfoxide)(1*H*-imidazole)ruthenate(III) (NAMI-A), indazolium *trans*-tetrachloridobis(1*H*-indazole)ruthenate(III) (KP1019), and sodium *trans*-tetrachlorido-bis(1*H*-indazole)ruthenate(III) (NKP-1339), which have entered phase II clinical trials [5,6,9,10,13–15]. Generally, treatment with Ru pharmaceuticals results in less severe side effects than those of platinum drugs [16,17]. Previously it was thought that, like many Pt drugs, drug interactions with blood components are detrimental to activity. However, research into Ru adducts with proteins and biological molecules have led to some drugs, such as NAMI-A and KP1019, to be classed as pro-drugs (meaning that the complexes must undergo biotransformations in the body to become active agents) [5,8,11,18–24]. This activation involves substitution of halido and other ligands under physiologically relevant conditions [5,8,11,18–24].

The macrocyclic ligand, 1,4,7-trithiacyclononane ([9]aneS<sub>3</sub>), occupies a face of octahedral metal centers to form stable

<sup>☆</sup> In honour of the Late Professor Karen J. Brewer.

<sup>\*</sup> Corresponding author.

E-mail address: [peter.lay@sydney.edu.au](mailto:peter.lay@sydney.edu.au) (P.A. Lay).

complexes [25]. Complexes of this type are attractive as potential anti-cancer pro-drugs as the strongly bound macrocycle leaves three coordination sites free for ligands to act as leaving groups for interactions with serum proteins.

Exploration of Ru complexes with the [9]aneS<sub>3</sub> ligand as potential cytotoxins [26–32] has uncovered some highly cytotoxic compounds. However, the anti-metastatic activity of Ru<sup>II</sup>-[9]aneS<sub>3</sub> complexes with the general formula [RuX<sub>2</sub>([9]aneS<sub>3</sub>)(S-dmsO)] (X = Cl, Br, I, Fig. 1) have yet to be explored until the current study.

## 2. Materials and methods

### 2.1. Synthesis

The reagents used were of analytical grade or higher. The following reagents were purchased from Sigma Aldrich and used as received: RuCl<sub>3</sub>·3H<sub>2</sub>O, RuBr<sub>3</sub> (anhydrous), 1,4,7-trithiacyclononane, thiazolyl blue tetrazolium bromide (MTT), dimethylsulfoxide (dmsO), Ru standard (1023 µg/mL in HCl), 4-(2-hydroxyethyl)-1-piperazineethanesulfonic acid (HEPES), phosphate buffered saline (PBS), iodoacetic acid, boron nitride, nitric acid (65% v/v), hydrochloric acid (37% v/v), hydrobromic acid (48% v/v), and potassium iodide.

NAMI-A [33,34], [RuCl<sub>2</sub>([9]aneS<sub>3</sub>)(S-dmsO)]·2H<sub>2</sub>O [35], [RuBr<sub>2</sub>(S-dmsO)<sub>4</sub>] [36], and [Ru<sub>2</sub>(S-dmsO)<sub>4</sub>] [24] were synthesized according to published procedures. Full details are included in the Supplementary Information together with the <sup>1</sup>H and <sup>13</sup>C NMR spectra of [RuCl<sub>2</sub>([9]aneS<sub>3</sub>)(S-dmsO)]·2H<sub>2</sub>O (Figs. S1 and S2, respectively).

#### 2.1.1. [RuBr<sub>2</sub>([9]aneS<sub>3</sub>)(S-dmsO)]

Freshly distilled ethanol (5 mL) was added to [RuBr<sub>2</sub>(S-dmsO)<sub>4</sub>] (119 mg, 0.208 mmol) and [9]aneS<sub>3</sub> (38.9 mg, 0.208 mmol), and the suspension was heated to reflux. After 10 min the solution turned orange and a bright orange solid was formed. Following a further 30 min of reflux, the solid was filtered and washed with freshly distilled ethanol (2 mL) and diethyl ether (2 mL), and dried in vacuo; yield 75.6 mg, 83.3 mmol, 70%. Anal. Calc. For RuBr<sub>2</sub>S<sub>4</sub>OC<sub>8</sub>H<sub>18</sub>: Calculated: C 18.50, H 3.49, Br 30.77; Found C 18.55, H 3.51, Br 30.75. UV/Vis: (H<sub>2</sub>O, 0.50 mM) 330 nm ( $\epsilon = 3.4 \times 10^2 \text{ M}^{-1} \text{ cm}^{-1}$ ), 370 nm ( $\epsilon = 3.5 \times 10^2 \text{ M}^{-1} \text{ cm}^{-1}$ ), 436 nm ( $\epsilon = 3.6 \times 10^2 \text{ M}^{-1} \text{ cm}^{-1}$ ). <sup>1</sup>H NMR (CD<sub>3</sub>Cl, Fig. S3)  $\delta = 3.51$  (s, 6 H)  $\delta = 2.41$ – $3.68$  (m, 12 H) ppm. <sup>13</sup>C NMR (CD<sub>3</sub>CN, Fig. S4)  $\delta = 45.71$  ((CH<sub>3</sub>)<sub>2</sub>S=O), 35.16, 32.92, 32.60 ([9]aneS<sub>3</sub>) ppm. FTIR (KBr, cm<sup>-1</sup>): 1444 vw, 1406 m, 1297 vw, 1088 s (ν SO), 1006 m, 963 w, 930 vw, 907 w, 831 vw, 819 vw, 717 m (ν CS)<sub>asym</sub>, 677 m (ν CS)<sub>sym</sub>, 528 vw, 510 vw, 501 vw, 493 vw, 482 vw, 460 vw, 442 vw, 421 vs (ν Ru-Br), 406 w, 401 w.

#### 2.1.2. [RuI<sub>2</sub>([9]aneS<sub>3</sub>)(S-dmsO)]·0.1EtOH

The pink brown solid [RuI<sub>2</sub>(S-dmsO)<sub>4</sub>] (185 mg, 0.28 mmol) and [9]aneS<sub>3</sub> (50 mg 0.28 mmol) were added to freshly distilled ethanol (10 mL) under an atmosphere of Ar for 20 min during which time a brown orange solid formed. The solid was filtered and washed with

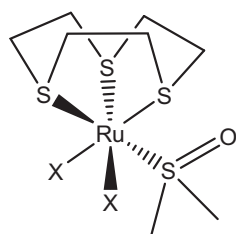


Fig. 1. Structure of [RuX<sub>2</sub>([9]aneS<sub>3</sub>)(S-dmsO)] (X = Cl, Br, I) complexes.

cold ethanol and diethyl ether and dried in vacuo; yield, 142 mg, 0.23 mmol, 96%. FTIR (KBr, cm<sup>-1</sup>) data: 1444 m, 1403 m, 1309 w, 1281 w, 1076 s, 1006 s, 962 w, 937 w, 923 m, 904 m, 822 m, 713 sh, 675 m, 528 w, 472 w, 426 m. Anal. Calc. For RuI<sub>2</sub>S<sub>4</sub>OC<sub>8</sub>H<sub>18</sub>·0.1EtOH: Calculated: C 15.94, H 3.03, I 41.07; Found C 16.12, H 2.96, I 41.26.

### 2.2. Elemental analysis

Non-metal elemental analyses were performed by the Microanalytical Unit, Research School of Chemistry, Australian National University.

### 2.3. Spectroscopy

UV/Vis spectra were recorded at 310 K using a Hewlett-Packard HP 8452 A diode-array spectrophotometer fitted with a Peltier temperature controller, using a 1-cm path length quartz cells. The spectra and the positions and extinction coefficients of the peaks for [RuX<sub>2</sub>([9]aneS<sub>3</sub>)(S-dmsO)] (X = Cl, Br) are contained in Fig. S5 and Table S1, respectively. For solid-state Fourier-transform infrared (FTIR) spectroscopy, samples were diluted with KBr and were recorded on a Bio-Rad FTS-40 spectrometer. The FTIR spectra and peak assignments for [RuX<sub>2</sub>([9]aneS<sub>3</sub>)(S-dmsO)] (X = Cl, Br) (Fig. S6, Table S2), Br (Fig. S7, Table S3) and I (Fig. S8, Table S4) are contained in the Supplementary Information.

Ru content was obtained by dissolving the sample in dmsO and then diluting with HCl (0.1 mM). The samples were measured by atomic absorption spectroscopy (AAS) with a GTA 120 Graphite Tube Atomizer, 299 Series AA. The data were calibrated against a Ru standard diluted in HCl (0.1 mM) to 500 ng/mL.

For <sup>1</sup>H NMR and <sup>13</sup>C NMR spectroscopies, Ru complexes were dissolved in D<sub>2</sub>O, CD<sub>3</sub>Cl, MeOD or CD<sub>3</sub>CN (Sigma Aldrich) and spectra were recorded on a Bruker AVANCE300 NMR Spectrometer. Chemical shifts ( $\delta$ , parts per million (ppm)) were referenced internally to tetramethylsilane (TMS) at 0 ppm. Spectra were collected with Bruker TopSpin 3.0 software [37], and processed with Spinworks 3.0 [38].

### 2.4. UV/Vis kinetics

Solutions of Ru complexes in dmsO (50 µL, 10 mM) were added to 950 µL of the following solutions immediately before analysis: fully supplemented Dulbecco's Modified Eagle Medium (DMEM, details of the components are contained in the Supplementary Information, Table S5), pH 7.4 with no added phenol red indicator; and HEPES buffer, pH 7.4.

After addition of Ru complexes to the solution, spectra were recorded at 310 K using a Hewlett-Packard HP 8452A diode-array spectrophotometer fitted with a Peltier temperature controller (wavelength range 200–700 nm). Spectra were recorded at regular intervals (1–500 s). Solutions were maintained at a constant temperature of 310 K for the duration of analysis. All experiments were performed in triplicate and analyses of kinetic data were performed with Pro-Kineticist I [39,40].

### 2.5. Biochemicals and cell lines

Collagen I (rat tail) was purchased from Life Technologies, and was used as received. Cell lines (human alveolar basal epithelial adenocarcinoma (A549), and human mammary gland epithelial adenocarcinoma (MDA-MB-231)) were received from the American Type Culture Collection (ATCC). Cell culture media and supplements were purchased from Invitrogen and used as received: DMEM, Glutamax, antibiotic-antimycotic mixture, (100 U/mL penicillin, 100 mg/mL streptomycin, 0.25 mg/mL amphotericin B), and

fetal calf serum. Bio-Gel P-30 spin columns (molecular mass cut-off, 30 kDa) were purchased from BioRad.

Cells were cultured in a monolayer in Advanced DMEM and supplemented with Glutamax (2.0 mM), antibiotic–antimycotic mixture, and fetal calf serum (heat inactivated, 2% v/v). Cells were seeded at a density of 30–40 cells/mm<sup>2</sup> and incubated in a 5% CO<sub>2</sub> humidified incubator at 310 K for 3–4 d until ≥80% confluent before sub-culturing.

## 2.6. X-ray absorption spectroscopy

### 2.6.1. Sample preparation

Stock solutions 10 mM were prepared for all compounds ([RuCl<sub>2</sub>([9]aneS<sub>3</sub>)(dmsO)], [RuBr<sub>2</sub>([9]aneS<sub>3</sub>)(dmsO)], and NAMI-A) in dmsO and were stored in the dark. The solutions were sufficiently stable for various studies for the time of storage (1–2 d in the dark), as was confirmed by UV/Vis spectroscopy. Samples of the products from the reactions of Ru complexes with fully supplemented Advanced DMEM, collagen (1.5 mg/mL in PBS, pH 7.4) and HEPES buffer were prepared by reactions of these media with Ru complexes (final concentration 0.50 mM). Samples were incubated at 310 K for 0, 1, 4, 8, or 24 h.

After the incubation with collagen, Ru-protein solutions were cooled to 277 K and unbound Ru was removed using Bio-Gel P-30 spin columns by gentle centrifugation (2000 rpm, 4 min, 277 K). To preserve the Ru environment following incubation, all solutions were immediately snap-frozen at 196 K [8,21,41]. The samples were stored at 196 K until they were freeze-dried under vacuum at ~223 K to both increase the Ru concentration of the sample by removal of water and minimize photodamage [41]. Samples of model Ru complexes were prepared by mixing solid compounds with boron nitride in ~1:10 mass ratio.

### 2.6.2. Data collection

The beam energy at the Photon Factory, Australian National Beamline Facility (ANBF) was 2.5 GeV, and the maximal beam current was 430 mA. A 311 double-crystal sagittally focusing monochromator was used. Neat freeze-dried samples or mixtures of model complexes with BN were pressed into a 0.5-mm thick cell that was between two 63.5 μm Kapton tape windows (window size, 2 × 10 mm<sup>2</sup>). Freeze-dried incubation/biological samples were collected over the *k* range of 0–14 Å<sup>-1</sup>, and Ru complexes were diluted in BN and XAS data were collected over the *k* range of 0–16 Å<sup>-1</sup>. All XAS were collected at 15–20 K (maintained with a Cryo Industries reverse cycle liquid He cryostat, which was flushed of air and maintained a under vacuum/He environment) in fluorescence detection mode, using a 36-pixel Ge planar detector (EurisyS). XAS samples were placed at an angle of 45° to the incident X-ray, and the Ge detector was placed at 90° to the incident X-ray. The spectra were recorded over the 21,900–22,900 eV energy range (pre-edge region, 21,900–22,080 eV with 9 eV steps; XANES region, 22,080–22,180 eV with 0.25 eV steps; and EXAFS region, 22,180–22,900 eV with 0.05 Å<sup>-1</sup> steps in *k*-space). The output of the incident and transmitted beams were normalized using ionization chamber, *I*<sub>0</sub>, and ionization chambers, *I*<sub>1</sub> and *I*<sub>2</sub> were used to determine the transmission XAS of the Ru foil standard. The ionization chamber *I*<sub>0</sub> contained N<sub>2</sub> and chambers *I*<sub>1</sub> and *I*<sub>2</sub> contained Ar. The energy scale was calibrated using the Ru foil; calibration energy, 22,117 eV, corresponded to the first peak of the first derivative of Ru<sup>0</sup> edge [42].

Between one and six scans were recorded for each sample and the absence of noticeable photodamage of the samples was confirmed from the lack of significant spectral changes between the scans (e.g., the difference in edge energies did not exceed 0.2 eV).

### 2.6.3. Data processing

Ru XAS data were processed using the EXAFSPAK software package [43]. The spectrum from each pixel of the Ge detector was examined and spectra with no or very little signal were excluded and multiple spectra were averaged and calibrated using the MAVÉ program. The spectra were averaged and calibrated (to 22,117 eV, corresponding to the first peak of the first derivative of Ru<sup>0</sup> edge) [41,42] using the MAVÉ program [43]. Normalization and background subtraction were performed using the BASKSUB program [43]. After background subtraction and normalization, the decay of the post edge region was fitted to the theoretical X-ray cross sections of Ru [44]. The data were converted to ASCII format using the PROCESS program for import into Origin Software for analysis [45].

## 2.7. Cell cytotoxicity, migration and invasion assays

The experimental methods for the MTT assay and determination of intracellular Ru content and their results are in the [Supplementary Information](#).

For migration assays, in a 96-well Essen Bioscience ImageLock™ plate, A549 cells were allowed to multiply over 3 d until cells in the wells were ~95% confluent. Uniform wounds were then made with an Essen 96 pin wound maker. The displaced cells were then removed by washing with serum free Advanced DMEM three times. Supplemented Advanced DMEM (reduced serum content of 0.8% v/v, to reduce cell proliferation, 100 μL) was added to each well with dmsO (with or without Ru complex) to a concentration of 1% v/v. The reagent plate was then placed in the InCuCyte™ Kinetic Imaging System located inside the cell incubator. Images of all wells were taken periodically at 2 h intervals for a period of 88 h. Individual images were chronologically collated and the relative wound density was calculated using InCuCyte™ Software Integrated Analysis Metrics [46]. Final results were expressed as a mean ± SD from three independent experiments.

For invasion assays, in a 96-well Essen Bioscience ImageLock™ plate, MDA MB 231 cells were allowed to multiply over 3 d until the cells in the wells were ~95% confluent. Uniform wounds were then made with an Essen 96 pin wound maker. The displaced cells were then removed by washing with serum free Advanced DMEM three times. Pre-chilled, neutralized collagen (1 mg/mL, 50 μL) with or without Ru, was carefully added to each well. Care was taken to avoid bubble formation. The plate was then put in an incubator (310 K, 5% CO<sub>2</sub>) for 30 min, to allow the collagen gel to set. Supplemented Advanced DMEM (reduced serum content of 0.8% v/v to reduce cell proliferation, 100 μL) was added to each well with dmsO (with or without Ru complex) to a concentration of 1% v/v. The reagent plate was then placed in the InCuCyte™ Kinetic Imaging System located inside the cell incubator. Images of all wells were taken periodically at 2 h intervals for a period of 88 h. Individual images were chronologically collated and the relative wound density was calculated using InCuCyte™ Software Integrated Analysis Metrics [46]. Final results were expressed as a mean ± SD from three independent experiments.

## 2.8. Statistics

Where necessary, two data sets were compared by a two-way analysis of variance with Origin® Software [45]. In this method, two data sets were tested to ascertain whether two groups are significantly different from each other, and the null hypothesis (that there is no difference other than chance between the two means) can be rejected [47–50]. When data sets were compared for significant difference, no presumption was made regarding the direction of the variance, i.e., non-directional analysis was used. Probability thresholds of *P* < 0.05, *P* < 0.01, and *P* < 0.001 are reported where a

minimum  $P < 0.05$  was required for a difference to be considered significant.

### 3. Results

#### 3.1. Synthesis

A series of Ru<sup>II</sup> complexes,  $[\text{RuX}_2(\text{[9]aneS}_3)(\text{S-dmsO})]$  with (X = Cl, Br, and I) were synthesized. All corresponding precursors,  $[\text{RuX}_2(\text{S-dmsO})_4]$ , were prepared from their corresponding Ru<sup>III</sup> halides and were characterized by elemental analysis (at a minimum) to ensure their purities before further reaction.

$[\text{RuBr}_2(\text{[9]aneS}_3)(\text{S-dmsO})]$  and  $[\text{RuI}_2(\text{[9]aneS}_3)(\text{S-dmsO})]$  syntheses were adapted from that of  $[\text{RuCl}_2(\text{[9]aneS}_3)(\text{S-dmsO})]$  [35]. However,  $[\text{RuI}_2(\text{[9]aneS}_3)(\text{S-dmsO})]$  proved to be insoluble in aqueous media and, therefore, was only characterized by elemental analysis and IR spectroscopy and the solubility prevented its use in the biological assays.  $[\text{RuCl}_2(\text{[9]aneS}_3)(\text{S-dmsO})]$  and  $[\text{RuBr}_2(\text{[9]aneS}_3)(\text{S-dmsO})]$  were characterized by elemental analysis, NMR, IR, UV/vis spectroscopies.

#### 3.2. Substitution kinetics in biological media

The reaction kinetics of  $[\text{RuX}_2(\text{[9]aneS}_3)(\text{S-dmsO})]$  (X = Cl, Br) in HEPES buffer and fully supplemented cell culture media were investigated by UV/vis spectroscopy at 310 K (Figs. 2–4). Their

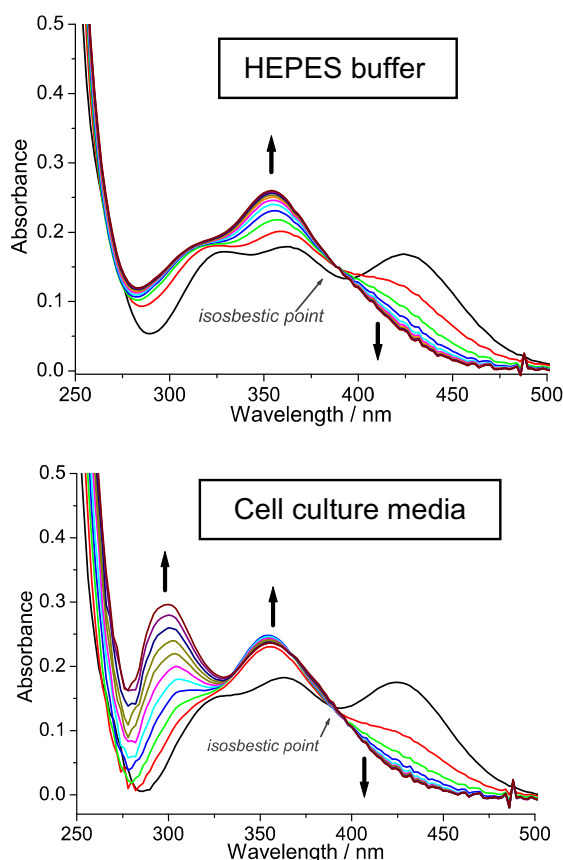


**Fig. 2.** TOP: reaction of 0.5 mM  $[\text{RuCl}_2(\text{[9]aneS}_3)(\text{S-dmsO})]$  in HEPES, pH 7.4 (310 K), spectra taken at 30 min time intervals. Initial peaks: 327 nm ( $\epsilon = 344 \text{ M}^{-1} \text{ cm}^{-1}$ ), 362 nm ( $\epsilon = 358 \text{ M}^{-1} \text{ cm}^{-1}$ ), 426 nm ( $\epsilon = 340 \text{ M}^{-1} \text{ cm}^{-1}$ ); New Peak: 353 nm ( $\epsilon = 518 \text{ M}^{-1} \text{ cm}^{-1}$ ). Isosbestic point: 389 nm ( $\epsilon = 298 \text{ M}^{-1} \text{ cm}^{-1}$ ). BOTTOM: Reaction of 0.5 mM  $[\text{RuCl}_2(\text{[9]aneS}_3)(\text{S-dmsO})]$  in cell culture media, pH 7.4 (310 K). Initial peaks: 327 nm ( $\epsilon = 302 \text{ M}^{-1} \text{ cm}^{-1}$ ), 362 nm ( $\epsilon = 365 \text{ M}^{-1} \text{ cm}^{-1}$ ), 426 nm ( $\epsilon = 353 \text{ M}^{-1} \text{ cm}^{-1}$ ). New Peaks: 299 nm ( $\epsilon = 594 \text{ M}^{-1} \text{ cm}^{-1}$ ), 355 nm ( $\epsilon = 498 \text{ M}^{-1} \text{ cm}^{-1}$ ). Isosbestic point: 389 nm ( $\epsilon = 264 \text{ M}^{-1} \text{ cm}^{-1}$ ).

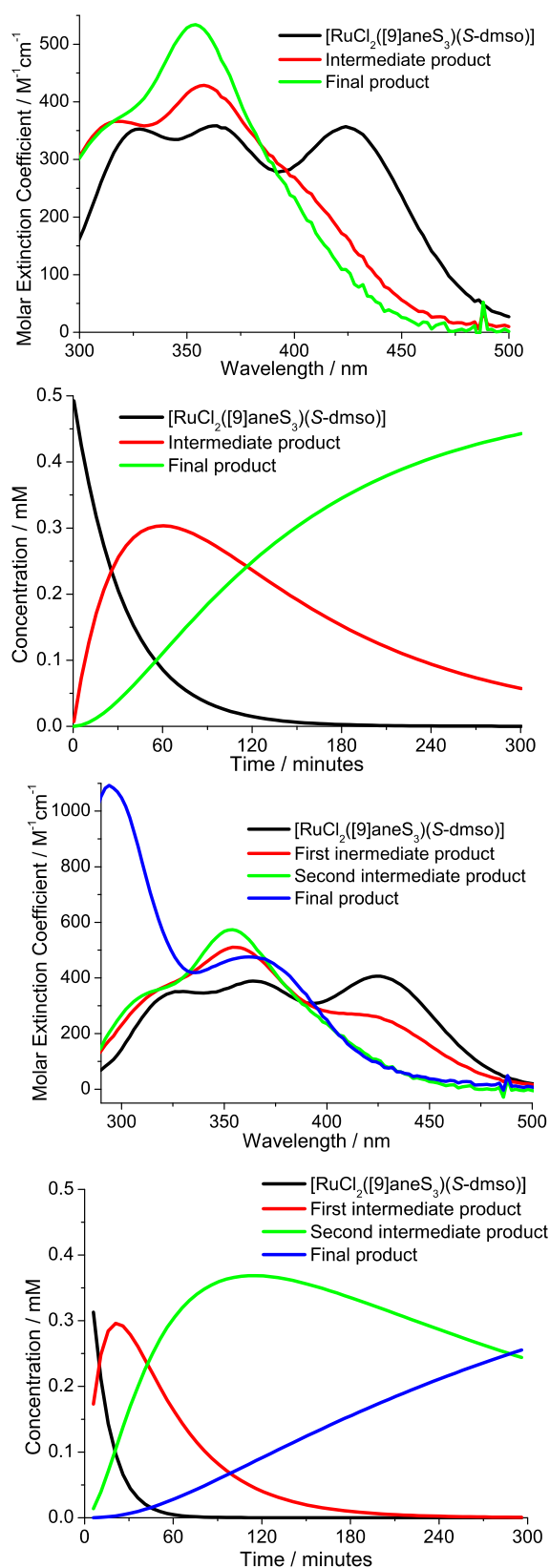


**Fig. 3.** Calculated spectra of species present in the reactions, and concentration profiles at 310 K from 0.50 mM  $[\text{RuCl}_2(\text{[9]aneS}_3)(\text{S-dmsO})]$  reactions in HEPES (top) and cell culture media (bottom), calculated by the use of global kinetic analysis from the data in Table 1.

electronic absorption spectra in both media featured two ligand-to-metal charge transfer (LMCT) bands at  $\sim 327$  nm and

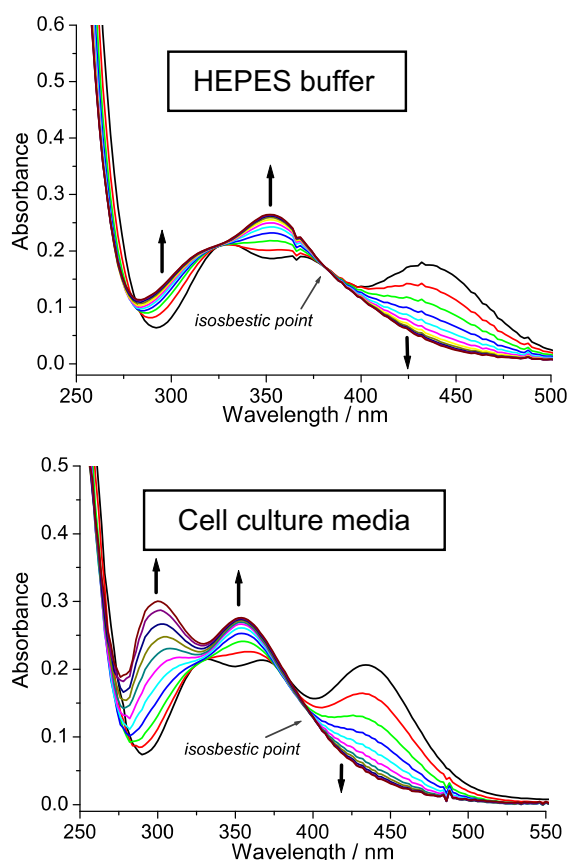


**Fig. 4.** TOP: reaction of 0.5 mM  $[\text{RuBr}_2([\text{9}]\text{aneS}_3)(\text{S-dmsO})]$  in HEPES, pH 7.4 (310 K), spectra taken at 30 min time intervals. Initial peaks: 327 nm ( $\epsilon = 420 \text{ M}^{-1} \text{ cm}^{-1}$ ), 367 nm ( $\epsilon = 378 \text{ M}^{-1} \text{ cm}^{-1}$ ), 426 nm ( $\epsilon = 354 \text{ M}^{-1} \text{ cm}^{-1}$ ). New Peak: 353 nm ( $\epsilon = 532 \text{ M}^{-1} \text{ cm}^{-1}$ ). Isosbestic point: 382 nm ( $\epsilon = 340 \text{ M}^{-1} \text{ cm}^{-1}$ ). BOTTOM: Reaction of 0.5 mM  $[\text{RuBr}_2([\text{9}]\text{aneS}_3)(\text{S-dmsO})]$  in cell culture media, pH 7.4 (310 K). Initial peaks: 327 nm ( $\epsilon = 232 \text{ M}^{-1} \text{ cm}^{-1}$ ), 370 nm ( $\epsilon = 426 \text{ M}^{-1} \text{ cm}^{-1}$ ), 435 nm ( $\epsilon = 414 \text{ M}^{-1} \text{ cm}^{-1}$ ). New Peaks: 300 nm ( $\epsilon = 604 \text{ M}^{-1} \text{ cm}^{-1}$ ), 354 nm ( $\epsilon = 554 \text{ M}^{-1} \text{ cm}^{-1}$ ). Isosbestic point: 398 nm ( $\epsilon = 270 \text{ M}^{-1} \text{ cm}^{-1}$ ).

$\sim 360 \text{ nm}$ . A third band at  $\sim 430 \text{ nm}$ , which represented the charge transfer band between Ru and Cl (for  $[\text{RuCl}_2([\text{9}]\text{aneS}_3)(\text{S-dmsO})]$ ) or Ru and Br (for  $[\text{RuBr}_2([\text{9}]\text{aneS}_3)(\text{S-dmsO})]$ ) was gradually lost over the time of incubation, which showed complete loss of the halido ligands. This change was accompanied by the formation of a new peak at  $\sim 353 \text{ nm}$  for both complexes in both HEPES and cell culture media. An additional new peak at  $\sim 300 \text{ nm}$  formed upon incubation of  $[\text{RuX}_2([\text{9}]\text{aneS}_3)(\text{S-dmsO})]$  ( $\text{X} = \text{Cl}, \text{Br}$ ) with fully supplemented cell culture media. An isosbestic point at 389 nm indicated a clean substitution reaction occurring during the incubation of  $[\text{RuCl}_2([\text{9}]\text{aneS}_3)(\text{S-dmsO})]$  with cell culture media; this isosbestic point included all but the first time point at 30 s. The isosbestic point for the reaction of  $[\text{RuBr}_2([\text{9}]\text{aneS}_3)(\text{S-dmsO})]$  in

cell culture media was shifted to 398 nm, and included all time points from 2 h of incubation.

Average rate constants (as determined by Global Analysis Pro-K software) are displayed in Table 1 [39]. Calculated spectra of the reactions of  $[\text{RuCl}_2([\text{9}]\text{aneS}_3)(\text{S-dmsO})]$  are shown in Fig. 3. Calculated spectra for  $[\text{RuBr}_2([\text{9}]\text{aneS}_3)(\text{S-dmsO})]$  and selected experimental and calculated kinetic curves for both complexes are detailed in the Supplementary Information (Figs. S9–S12).

The reaction kinetics of  $[\text{Ru}_2([\text{9}]\text{aneS}_3)(\text{S-dmsO})]$  ( $\text{X} = \text{Cl}, \text{Br}$ ) in HEPES buffer were fitted to two consecutive pseudo-first-order steps, whereas the reactions in cell culture media exhibited three consecutive pseudo-first-order reactions leading the final product.

The calculated spectra and concentration profiles are shown in Fig. 3 and the Supplementary Information (Figs. S11 and S12). The substitution rate constants for  $[\text{RuCl}_2([\text{9}]\text{aneS}_3)(\text{S-dmsO})]$  were 2.7, and 2.5 times higher for steps 1 and 2, respectively, than the corresponding rate constants of  $[\text{RuBr}_2([\text{9}]\text{aneS}_3)(\text{S-dmsO})]$  (Table 1). The rate constants for the formation of the final product (Step 3,  $k_3$ ), which only occurred in the biological media, were not statistically different between the two pro-drugs, and are presumed to correspond to the same reaction with a common intermediate.

Scheme 1 summarizes the Ru reactions in HEPES buffer and cell culture media. The pathway of halido aquation reactions is shown in black, and the additional possible reactions of protein binding are in grey. As expected, the final products for  $[\text{RuX}_2([\text{9}]\text{aneS}_3)(\text{S-dmsO})]$  ( $\text{X} = \text{Cl}, \text{Br}$ ) were the same, and corresponded to the substitution of both halido ligands. The two steps that occurred in HEPES buffer and the first two processes that occurred in cell culture media were the stepwise substitutions of the halido ligands. The rate constants were smaller for the bromido compared to chlorido ligands (Table 1).

### 3.3. XAS studies on the bio-transformations of Ru drugs

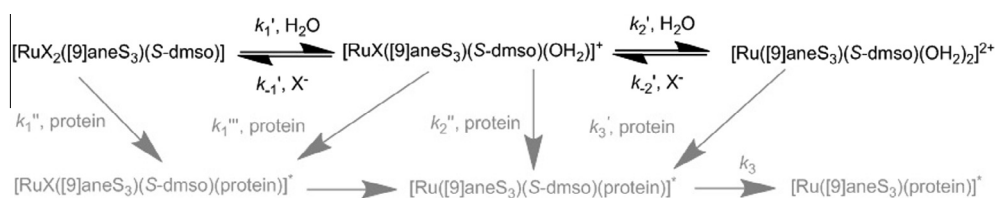
XAS spectra of the freeze-dried products from the reactions of  $[\text{RuX}_2([\text{9}]\text{aneS}_3)(\text{S-dmsO})]$  ( $\text{X} = \text{Cl}, \text{Br}$ ) with fully supplemented cell culture media (Advanced DMEM) are shown in Figs. 5 and 6, respectively. There were differences in the XAS of all reaction products in cell culture media compared to those of the parent pro-drugs. The most evident changes were in the white-line height, and second XAS peak.  $[\text{RuCl}_2([\text{9}]\text{aneS}_3)(\text{S-dmsO})]$  underwent a complete reaction after 4 h,  $[\text{RuBr}_2([\text{9}]\text{aneS}_3)(\text{S-dmsO})]$ , continued to show XAS spectral differences and a continued reaction at both the 4 h and 24 h reaction time points, although the differences between 4 and 24 h time points were minimal. Very similar XAS spectra and, therefore, Ru environments, were observed after 24 h incubation in cell culture media with  $[\text{RuX}_2([\text{9}]\text{aneS}_3)(\text{S-dmsO})]$  ( $\text{X} = \text{Cl}, \text{Br}$ , Fig. S13).

XAS speciation of Ru was studied for different incubation times for the reactions of the pro-drugs with a collagen gel that was set in cell culture media, pH 7.4. The XAS of the reaction products of  $[\text{RuX}_2([\text{9}]\text{aneS}_3)(\text{S-dmsO})]$  ( $\text{X} = \text{Cl}, \text{Br}$ ) with collagen after 1, 4 and 24 h are shown in Figs. 7 and 8, respectively. Different Ru

**Table 1**  
Pseudo first-order rate constants for substitution of Ru pro-drugs in biological media.<sup>a</sup>

Complex	Step	HEPES ( $\text{s}^{-1}$ )	Cell culture media ( $\text{s}^{-1}$ )
$[\text{RuCl}_2([\text{9}]\text{aneS}_3)(\text{S-dmsO})]$	$k_1(\text{obs})$	$(4.5 \pm 0.2) \times 10^{-4}$	$(1.3 \pm 0.1) \times 10^{-3}$
	$k_2(\text{obs})$	$(1.5 \pm 0.1) \times 10^{-4}$	$(5.0 \pm 0.5) \times 10^{-4}$
	$k_3(\text{obs})$	–	$(3.6 \pm 0.7) \times 10^{-5}$
$[\text{RuBr}_2([\text{9}]\text{aneS}_3)(\text{S-dmsO})]$	$k_1(\text{obs})$	$(2.6 \pm 0.2) \times 10^{-4}$	$(4.7 \pm 0.2) \times 10^{-4}$
	$k_2(\text{obs})$	$(9.2 \pm 0.1) \times 10^{-5}$	$(2.0 \pm 0.1) \times 10^{-4}$
	$k_3(\text{obs})$	–	$(3.9 \pm 0.3) \times 10^{-5}$

<sup>a</sup> Ru complexes  $[\text{RuX}_2([\text{9}]\text{aneS}_3)(\text{S-dmsO})]$  ( $\text{X} = \text{Cl}, \text{Br}$ ) and were reacted in fully supplemented cell culture media (Section 2.5) and HEPES buffer at 310 K, pH 7.4. Spectra were analyzed with Pro-K software, and the results are expressed as the mean  $\pm$  SD of three replicates.



**Scheme 1.** Reaction substitution pathways of  $[\text{RuX}_2([\text{9}]\text{aneS}_3)(\text{S-dmso})]$  ( $\text{X} = \text{Cl, Br}$ ). The  $k_1(\text{obs})$  values include contributions from the rate constants,  $k_1'$ ,  $k_1''$ ,  $k_1'''$  and  $k_{-1}'$  and  $k_2(\text{obs})$  from  $k_2'$ ,  $k_2''$ , and  $k_{-2}'$ . The reactions with rate constant,  $k_3$ , only occur in biological media. \*The charge of Ru complexes with protein adducts are uncertain.

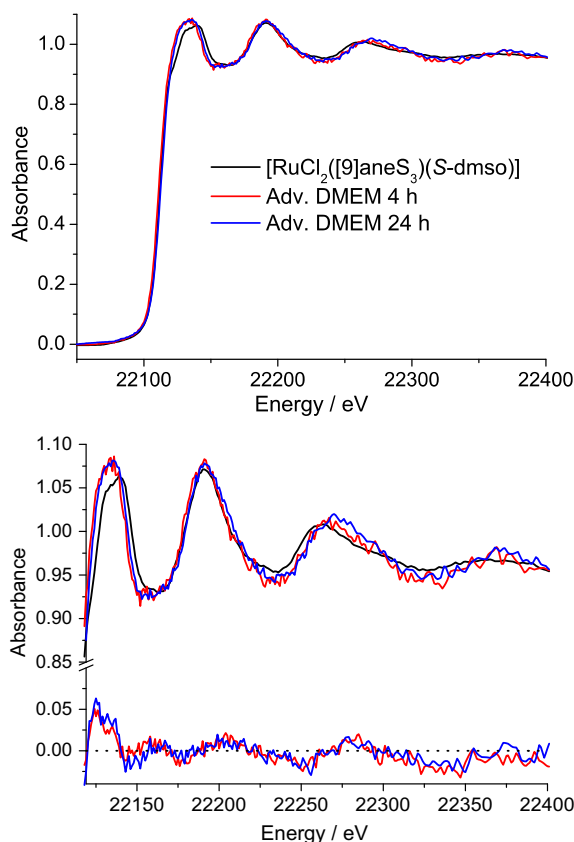


**Fig. 5.** Ru K-edge XAS of reaction products of  $[\text{RuCl}_2([\text{9}]\text{aneS}_3)(\text{S-dmso})]$  (0.5 mM) in supplemented Adv. DMEM (310 K, pH 7.4) after 4 h (red), and 24 h (blue) compared to the parent complex (black). TOP: full spectrum, BOTTOM: close up of XAS oscillations and difference spectra compared to the EXAFS of the parent complex. Freeze drying temperature, 223 K; measurement temperature, 10–20 K. (For interpretation of the references to colour in this figure legend, the reader is referred to the web version of this article.)

speciation was observed from the XAS of  $[\text{RuBr}_2([\text{9}]\text{aneS}_3)(\text{S-dmso})]$ , between the data obtained after 1 or 4 h of incubation, after which time the reaction was complete. This was consistent with the kinetic data for the first two steps. For  $[\text{RuCl}_2([\text{9}]\text{aneS}_3)(\text{S-dmso})]$ , the XAS changes indicated Ru speciation was complete after a single hour of incubation with the set collagen. As in cell culture media, very similar XAS speciation and, therefore, similar Ru environments, were observed for reactions of  $[\text{RuCl}_2([\text{9}]\text{aneS}_3)(\text{S-dmso})]$  and  $[\text{RuBr}_2([\text{9}]\text{aneS}_3)(\text{S-dmso})]$  with collagen after 24 h incubation (Fig. S14) but were somewhat different to those observed in cell medium.

### 3.4. Anti-cancer properties

Like NAMI-A [8], neither  $[\text{RuCl}_2([\text{9}]\text{aneS}_3)(\text{S-dmso})]$  nor  $[\text{RuBr}_2([\text{9}]\text{aneS}_3)(\text{S-dmso})]$  demonstrated any significant cytotoxicities against A549 human lung cancer cells (details in the

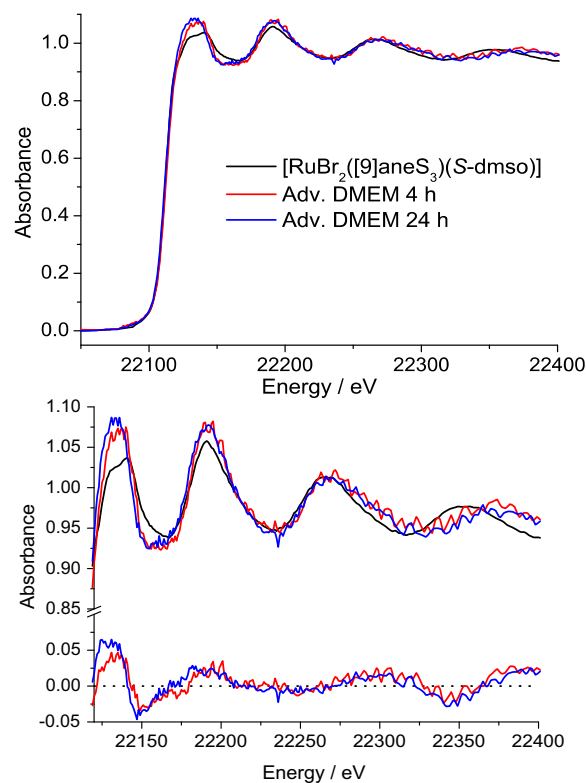


**Fig. 6.** Ru K-edge XAS of reaction products of  $[\text{RuBr}_2([\text{9}]\text{aneS}_3)(\text{S-dmso})]$  (0.5 mM) in supplemented Adv. DMEM (310 K, pH 7.4) after 4 h (red), and 24 h (blue) compared to the parent complex (black). TOP: full spectrum, BOTTOM: close up of XAS oscillations and difference spectra compared to the EXAFS of the parent complex. Freeze drying temperature, 223 K; measurement temperature, 10–20 K. (For interpretation of the references to colour in this figure legend, the reader is referred to the web version of this article.)

Supplementary Information, Fig. S15). Both caused an apparent reduction in migration of A549 cells but this was only significant for the chlorido complex (Fig. 9). While the migration assay indicated some anti-metastatic behavior for the chlorido complex, anti-invasive assays were also investigated for these complexes, along with the known metastasis inhibitor, NAMI-A, as a positive control.

MDA MB 231 cells were selected for collagen invasion assays instead of the A549 cells, because the MDA MB 231 cells are highly invasive as a result of expression of elevated levels of pro-invasive genes [51]. In the invasion assays described herein, the layer of collagen gel was set on top of a 2D cell culture following wound creation. The Ru pro-drug was applied either to the new collagen gel that set on top of the original layer of collagen and cells, or as a 24-h pre-treatment prior to wound creation and the addition of further untreated collagen. Invasion assays were used to determine the efficacy of the Ru pro-drugs on reducing the ability of MDA-MB-231 cells to invade into collagen across a wound. In invasion assays, the 3D collagen matrix surrounded the cells, and the

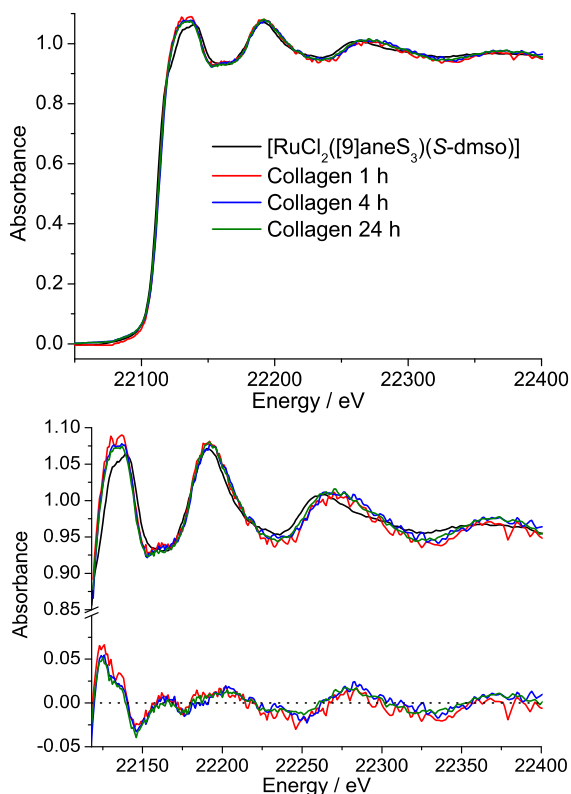


**Fig. 7.** Ru K-edge XAS of the reaction products of 0.5 mM  $[\text{RuCl}_2([\text{9}]\text{aneS}_3)(\text{S-dmsO})]$  in collagen gel (1 mg/mL, 310 K, pH 7.4) after 1 (red), and 4 (blue) and 24 (green) h, compared to parent pro-drug (black). TOP: full XAS; BOTTOM: close-up of XAS oscillations and difference spectra compared to that of the parent complex. Freeze-drying temperature, 223 K; measurement temperature 10–20 K. (For interpretation of the references to colour in this figure legend, the reader is referred to the web version of this article.)

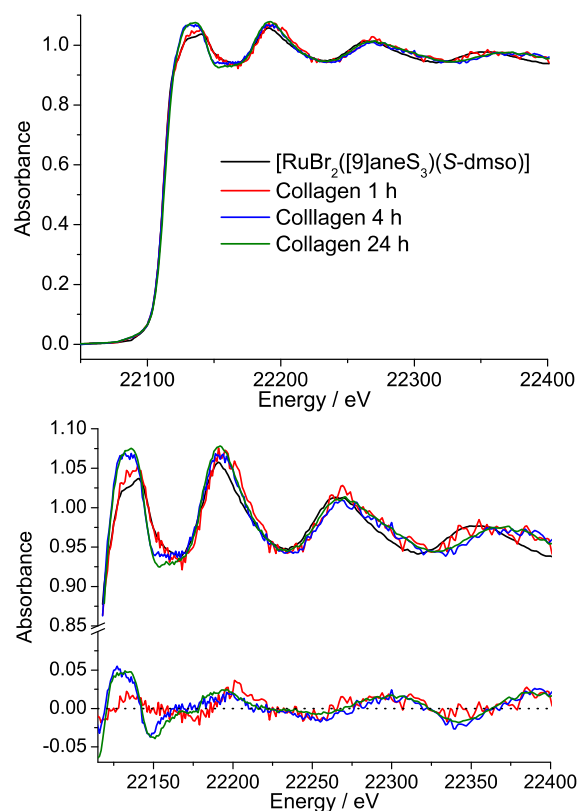


**Fig. 8.** Ru K-edge XAS of the reaction products of 0.5 mM  $[\text{RuBr}_2([\text{9}]\text{aneS}_3)(\text{S-dmsO})]$  in collagen gel (1 mg/mL, 310 K, pH 7.4) after 1 (red), and 4 (blue) and 24 h (green), compared to parent pro-drug (black). TOP: full XAS. BOTTOM: close-up of XAS oscillations and difference spectra compared to that of the parent complex. Freeze-drying temperature, 223 K; measurement temperature, 10–20 K. (For interpretation of the references to colour in this figure legend, the reader is referred to the web version of this article.)

localized points of integrin-facilitated adhesion observed in 2D migration, are replaced by matrix cell adhesions over the entire surface of the cell [52,53]. These 3D adhesions are more numerous, but their adhesive strength is much lower than for 2D attachment [54]. To invade, actomyosin contractility facilitates protrusion into collagen matrix where new adhesions are formed and proteolysis breaks adhesions at the ‘back’ of the cell [52–54]. The process of invasion is, therefore, very much dependent on morphodynamic changes to the cell, and the ability of Ru pro-drugs to inhibit these changes was examined in invasion assays. The elongation and formation of filopodia (in the direction of movement), of the cells invading into collagen was observed in these assays (Fig. 10). The use of invasion assays also allowed for twin experiments, where the effects of dosing the collagen gel, or pre-treating cells could be compared. Representative images of both types of invasion assays are shown in Fig. 11. These images show the varying extent of cell invasion under different treatment. Figs. 12 and S16 show the relative wound density versus time for Ru treated cells and collagen, respectively. For both types of Ru treatment,  $[\text{RuCl}_2([\text{9}]\text{aneS}_3)(\text{S-dmsO})]$  showed superior activity to  $[\text{RuBr}_2([\text{9}]\text{aneS}_3)(\text{S-dmsO})]$ .

Consistent with the similar effects on cancer cell migration and invasion for NAMI-A and  $[\text{RuCl}_2([\text{9}]\text{aneS}_3)(\text{S-dmsO})]$  is that after a 24 h treatment at 100  $\mu\text{M}$  Ru, they both have the same uptake of Ru of  $20 \pm 2$  and  $19 \pm 3$  ng Ru per million cells, respectively (see Supporting Information for experimental details). In addition, the distribution between the nuclear and non-nuclear fractions is similar with the total content in the cell membrane and cytoplasm being a factor of  $5.3 \pm 0.7$  and  $7 \pm 1$  higher for

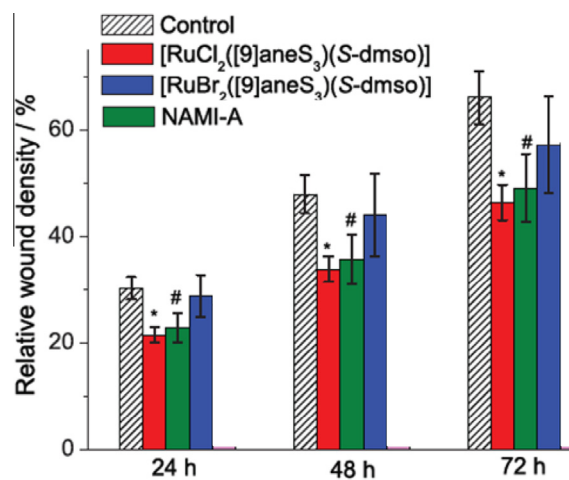


**Fig. 9.** Migration assay for Ru-treated A549 cells (100  $\mu\text{M}$  Ru in 1% dmsO; incubation conditions: 310 K, 5%  $\text{CO}_2$ ). Results are expressed as relative wound density at 24, 48 and 72 h. Data are expressed as the mean result of triplicate experiments  $\pm$  SD. (\* =  $P < 0.05$ , # =  $P < 0.15$ ).

$[\text{RuCl}_2([\text{9}]\text{aneS}_3)(\text{S-dmsO})]$  and NAMI-A, respectively. While  $[\text{RuBr}_2([\text{9}]\text{aneS}_3)(\text{S-dmsO})]$  also has a similar distribution ratio at  $6 \pm 1.5$ , less total Ru total is bound to cells;  $10 \pm 2$  ng Ru per million cells. This is consistent with the lower activity of the bromido complex and its slower substitution kinetics.

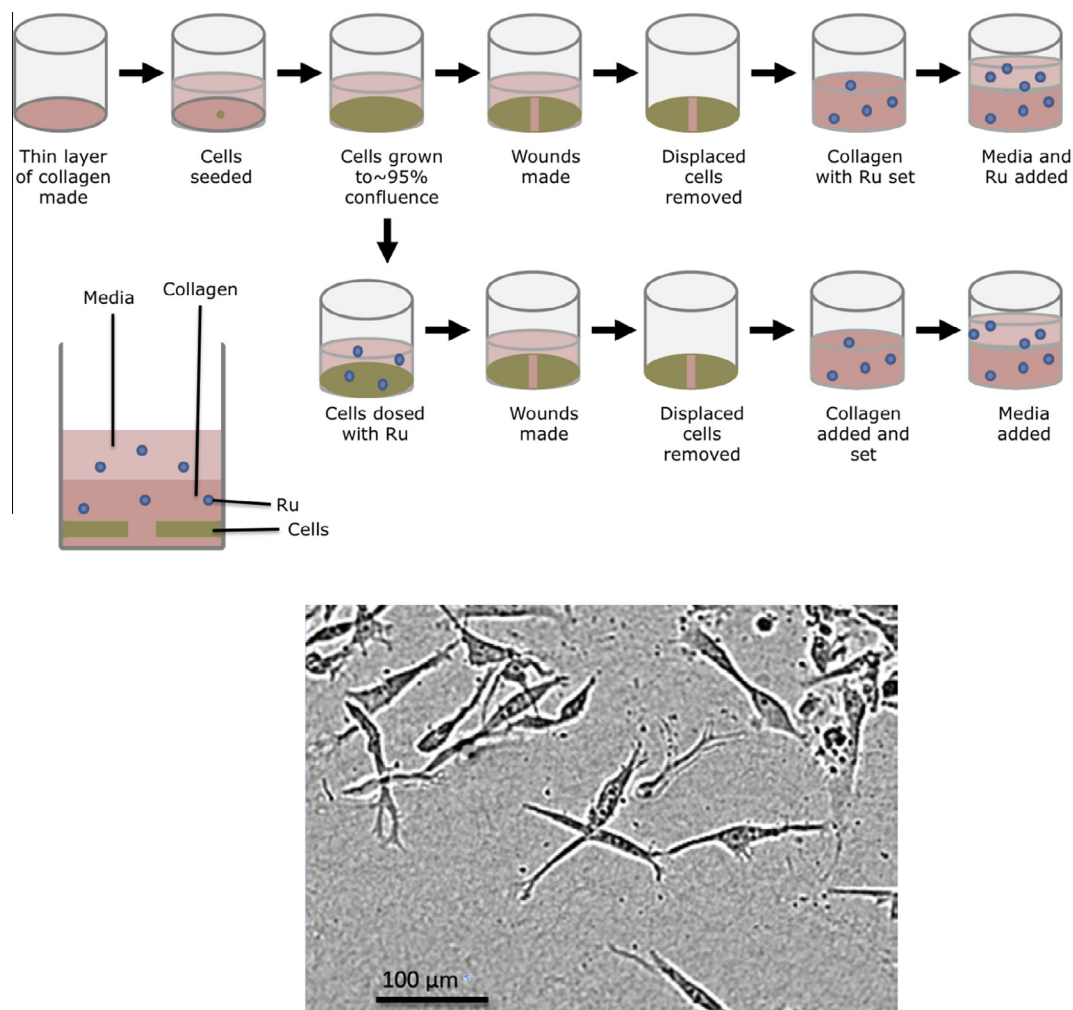


**Fig. 10.** TOP: experimental setup for cell invasion assays. BOTTOM: invading control (dmsol treated) MDA-MB-231 cells. A wound was made across ~90% confluent cells, and collagen was set on top of the cells. The cells were allowed to move into the free space. This image represents typical morphologies of invading MDA-MB-231 cells.

## 4. Discussion

### 4.1. Substitution reactions

The importance of the rates of halido substitution reactions on the anti-cancer properties of the  $[\text{RuX}_2(\text{[9]aneS}_3)(\text{S-dmsol})]$  ( $\text{X} = \text{Cl, Br}$ ) complexes has been investigated. As there is agreement in the literature that many Ru drugs interact with other biomolecules before they reach cancerous tissue, the kinetics of halido substitution of Ru complexes, such as Ru-arene complexes, NAMI-A and KP1019 have been studied previously [20,55–57]. Hypotheses have been made of the link between the substitution rates and *in vivo* activity [7,58]. In this work the kinetics of substitution of  $[\text{RuX}_2(\text{[9]aneS}_3)(\text{S-dmsol})]$  ( $\text{X} = \text{Cl, Br}$ ) in HEPES buffer and cell culture media at 310 K were investigated. Unfortunately, the iodo analogue was not sufficiently soluble to include in these studies. The chlorido complex was generally a factor of 2–3 times more reactive than the bromido complex. Since the chlorido complex had stronger anti-invasive effects than the bromido complex, it showed that substitution reactions were critical to biological activity. Moreover, it indicated that extracellular and/or interactions with the cell surface were most important in the anti-cancer activities. If intracellular process were more important, then the bromido complex would be expected to more active, since it has a greater lifetime in the medium. This would enable a longer period of time for passive diffusion of the neutral parent drug into the cells.

The natures of the substitution reactions were also informative. While the rates of substitution for the bromido complex were slower than the chlorido complex in  $[\text{RuX}_2(\text{[9]aneS}_3)(\text{S-dmsol})]$  ( $\text{X} = \text{Cl, Br}$ ), both followed sequential first order reactions involving two equation steps. The nature of the substitution reactions were established by the progressive loss of the Ru-X charge transfer bands in the UV/Vis spectra that were also consistent with shifts in the XAS edge and the observation of a common final product  $[\text{Ru}(\text{[9]aneS}_3)(\text{S-dmsol})(\text{OH}_2)_2]^{2+}$ . Even though such complexes could partially deprotonate to form an aqua/hydroxido complex,  $[\text{Ru}(\text{OH})(\text{[9]aneS}_3)(\text{S-dmsol})(\text{OH}_2)]^+$  all of these species are charged and would have slower passive diffusion into cells than the uncharged parent drug.

However, the kinetic studies in Advanced DMEM suggested that aqua species were unlikely to be present in significant concentrations in cell medium. The kinetic data obtained from UV/Vis spectroscopy were fitted to three consecutive pseudo-first-order reactions. As before, the first two reactions were consistent with the consecutive loss of the two halido ligands. However, the observation that the substitution reactions were faster in Advanced DMEM than in HEPES buffer at the same temperature and pH value were initially somewhat surprising, for two reasons. The first is that halido substitution from low-spin  $d^6$  Ru(II) is expected to occur via a dissociative interchange ( $I_d$ ) mechanism [59–61]. The second is that there is no added  $\text{Cl}^-$  to the HEPES, whereas the  $[\text{Cl}^-]_{\text{tot}}$  in cell culture media is 127 mM from  $\text{CaCl}_2$ ,  $\text{MgCl}_2$ ,  $\text{KCl}$ ,

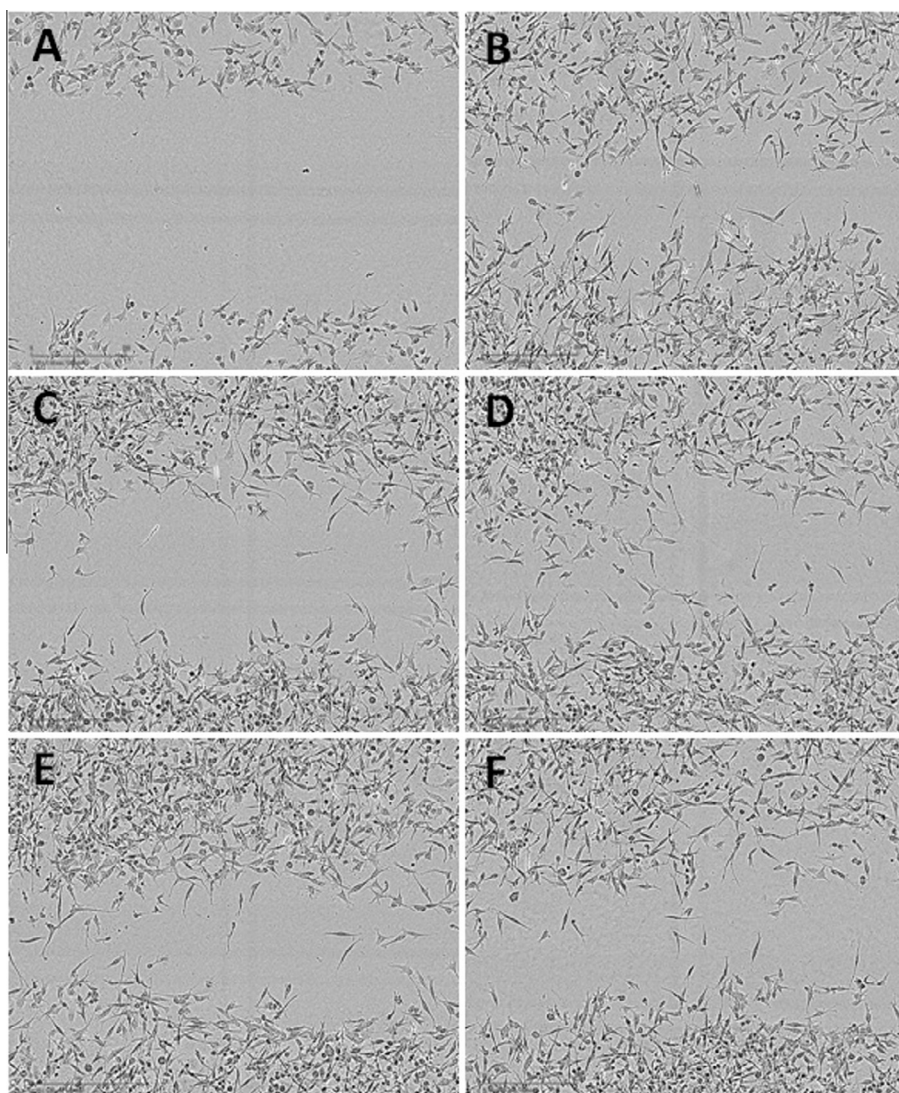


**Fig. 11.** Images of invading MDA-MB-231 cells. Control cells A: 0 h, B: 48 h, C:  $[\text{RuCl}_2(\text{[9]aneS}_3)(\text{S-dmsO})]$ -treated cells 48 h, D:  $[\text{RuCl}_2(\text{[9]aneS}_3)(\text{S-dmsO})]$ -treated collagen and media 48 h, E:  $[\text{RuBr}_2(\text{[9]aneS}_3)(\text{S-dmsO})]$ -treated cells 48 h, F:  $[\text{RuBr}_2(\text{[9]aneS}_3)(\text{S-dmsO})]$ -treated collagen and media 48 h.

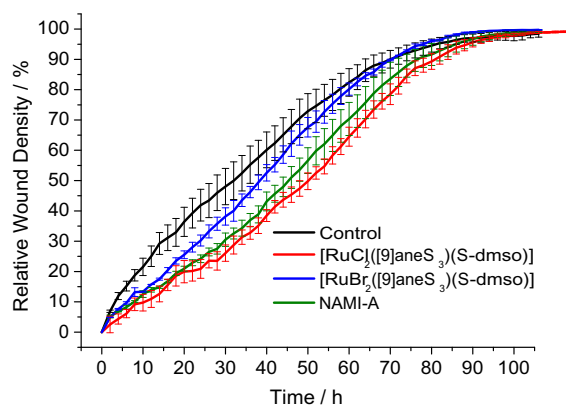


**Fig. 12.** Invasion assays for control,  $[\text{RuX}_2(\text{[9]aneS}_3)(\text{S-dmsO})]$  ( $\text{X} = \text{Cl}, \text{Br}$ ), and NAMI-A treated MDA-MB-231 cells ( $100 \mu\text{M Ru}$  in 1% dmsO, incubation conditions: 310 K, 5%  $\text{CO}_2$ ). Results are expressed as relative wound density vs. time after wound creation.

and NaCl [62]. Therefore, the reverse anation reaction would be expected to result in pseudo-first order rate constants that were smaller in Advanced DMEM, not larger.

These observations can be explained by the following. The rate constants of substitution reactions in  $I_d$  mechanisms depend on the incoming nucleophiles since there is some bond making in the transition state [59–61]. Certain nitrogen donors, such as imidazoles, as well as carboxylato and thiolato donors, are expected to be better nucleophiles than aqua ligands, especially if the pro-drug is already interacting with the biomolecule in question. For instance, serum proteins, such as serum albumin, readily bind and carry neutral molecules. NAMI-A and KP1019 bind to proteins in an intact form and undergo substitution reactions with protein pockets [23,63]. Therefore, the difference in rates of substitution could also be influenced by the difference in the environment within a protein.

The natures of the reactions in Advanced DMEM were consistent with the following observations. The first was that the calculated UV/Vis spectra from the global kinetic analysis after halido substitution were the same, as were the XAS at a similar stage of the reaction. This is consistent with the sequential loss of the halido ligands. It is postulated that the final reaction involves substitution of the dmsO ligand in cell medium, with the trithia macrocycle remaining bound. This third substitution reaction does not occur in buffered aqueous solution. This postulate is supported

by detailed studies of the speciation of these complexes in a range of biological media [11], using similar approaches as discussed previously [21]. These will be reported in subsequent publications.

The XAS of the adducts of  $[\text{RuX}_2(\text{[9]aneS}_3)(\text{S-dmsO})]$  ( $\text{X} = \text{Cl, Br}$ ) with collagen were different to those in Advanced MEM but they had the same XAS in the final product in a given medium, which was consistent with the loss of both halido ligands. Hence, the final speciation for both complexes was the same at 24 h in collagen.

#### 4.2. Anti-cancer activities

While the complexes were not cytotoxic they exhibited good anti-invasive activity with highly invasive MDA-MB-231 breast cancer cells. The molecular mechanisms that facilitate cell invasion are essential in mammals for several normal processes, such as wound healing, vascularisation, invasion, and neurite outgrowth [53]. In non-cancerous tissue, this process is strictly controlled and discontinues on the deprivation of physiological stimulus [1,53,64]. This tight regulation of invasion, that is characteristic of healthy cells, is not maintained in malignant tissue and this is the chief characteristic responsible for the spread of cancer from the primary tumor to other organs [64]. Further work exploring the full range of anti-cancer properties of these complexes needs to be performed; however, the invasion assays discussed here provided a strong indication of their anti-cancer potential and characteristics.

In the current studies, the abilities to limit invasion demonstrated by  $[\text{RuX}_2(\text{[9]aneS}_3)(\text{S-dmsO})]$  ( $\text{X} = \text{Cl, Br}$ ) were comparable and with those of NAMI-A. NAMI-A is well-known for anti-metastatic properties in *in vitro* assays and animal studies [7,8,10,65,66]. For the invasion experiments, (with long times of exposure of Ru to the cells/collagen to make up for the slower substitution kinetics of  $[\text{RuBr}_2(\text{[9]aneS}_3)(\text{S-dmsO})]$ ,  $[\text{RuCl}_2(\text{[9]aneS}_3)(\text{S-dmsO})]$  still had superior anti-metastatic efficacy. From these experiments, it was clear that the rate of ligand exchange is a vital predictor for *in vitro* cell activity. In this case, the slower reacting complex,  $[\text{RuBr}_2(\text{[9]aneS}_3)(\text{S-dmsO})]$ , had the same mode of action as  $[\text{RuCl}_2(\text{[9]aneS}_3)(\text{S-dmsO})]$ , but was inferior in anti-invasive ability, which was consistent with earlier predictions that the more reactive species were likely to have the strongest anti-invasive efficacies [7,19]. The observations that either treatment of the cells with the Ru complex for 24 h prior to adding the top collagen, or treatment of the top collagen after it had been applied to the existing layer of collagen and untreated cells, resulted in similar anti-invasion activities is important. It is consistent with our predictions that the main mechanism for anti-metastatic activities derives from reactions with the extracellular matrix and the cell surface [7,8,19,21] This also supports other evidence that Ru-transferrin transport mechanisms are not involved in the activities of these Ru complexes [67], since transport into cells does not appear to be important for this activity.

#### 5. Conclusions

In summary, this research has shown that the rate of ligand substitution in biological media has a key role in the mechanism of action, and efficacy of anti-invasive Ru complexes. For the two  $\text{Ru}^{\text{II}}$  complexes studied here, it is clear that a rate of substitution that is too slow can inhibit formation of vital Ru-protein interactions and lower the anti-metastatic activity.

Further research with a variety of related complexes may lead to the determination of structure-activity relationships that provide optimal rate constants for ligand substitution to maximize  $[\text{RuX}_2(\text{[9]aneS}_3)(\text{S-dmsO})]$  ( $\text{X} = \text{Cl, Br}$ ) *in vitro* anti-cancer efficacy.

It is also essential in future work, to determine whether these trends translate into *in vivo* efficacy.

#### Acknowledgements

This research was supported by an Australian Postgraduate Award to HAO and Australian Research Council Discovery and LIEF Grants to PAL (DP0984722, including a Professorial Fellowship, DP1095310, DP130103566, DP140100176, LE0346515 for the 36-pixel Ge detector, and LE110100174 for the international synchrotron access program of the Australian Synchrotron to travel to the Photon Factory). The authors acknowledge the facilities, and the scientific and technical assistance, of the Australian Microscopy & Microanalysis Research Facility at the Australian Centre for Microscopy and Microanalysis, The University of Sydney and the Bosch Institute, The University of Sydney. XAS measurements were performed at the ANBF (operated by the Australian Synchrotron) with the assistance of Dr. Michael Cheah, and Dr. Katherine Spiers. XAS data collection was carried out with the assistance of Dr. Zhi Jun Lim, Dr. Michelle Wood, and Dr. Nguyen Pham.

#### Appendix A. Supplementary data

Supplementary data associated with this article can be found, in the online version, at <http://dx.doi.org/10.1016/j.ica.2016.07.050>.

#### References

- [1] A. Jemal, E. Ward, Y.P. Hao, M. Thun, *J. Am. Med. Assoc.* 294 (2005) 1255–1259.
- [2] A. Bergamo, A. Masi, A.F.A. Peacock, A. Habtemariam, P.J. Sadler, G. Sava, *J. Inorg. Biochem.* 104 (2010) 79–86.
- [3] A. Jemal, R. Siegel, J.Q. Xu, E. Ward, *CA Cancer J. Clin.* 60 (2010) 277–300.
- [4] E. Alessio, G. Mestroni, A. Bergamo, G. Sava, *Curr. Top. Med. Chem.* 4 (2004) 1525–1535.
- [5] L.S. Flocke, R. Trondl, M.A. Jakupec, B.K. Keppler, *Invest. New Drugs* 34 (2016) 261–268.
- [6] S. Leijen, S.A. Burgers, P. Baas, D. Pluim, M. Tibben, E. van Werkhoven, E. Alessio, G. Sava, J.H. Beijnen, J.H.M. Schellens, *Invest. New Drugs* 33 (2015) 201–214.
- [7] A. Levina, A. Mitra, P.A. Lay, *Metalomics* 1 (2009) 458–470.
- [8] M.M. Liu, Z.J. Lim, Y.Y. Gwee, A. Levina, P.A. Lay, *Angew. Chem. Int. Ed.* 49 (2010) 1661–1664.
- [9] R. Trondl, P. Heffeter, C.R. Kowol, M.A. Jakupec, W. Berger, B.K. Keppler, *Chem. Sci.* 5 (2014) 2925–2932.
- [10] A. Bergamo, G. Sava, *Chem. Soc. Rev.* 44 (2015) 8818–8835.
- [11] H.A. O'Riley, Mechanisms of the anti-metastatic and cytotoxic properties of ruthenium anti-cancer drugs (Ph.D.), The University of Sydney, 2015.
- [12] A. Bergamo, A. Masi, M.A. Jakupec, B.K. Keppler, G. Sava, *Met. Based Drugs* (2009) 681270.
- [13] L. Bratsos, S. Jedner, T. Gianferrara, E. Alessio, *Chimia* 61 (2007) 692–697.
- [14] J.M. Rademaker-Lakhai, D. van den Bongard, D. Pluim, J.H. Beijnen, J.H.M. Schellens, *Clin. Cancer Res.* 10 (2004) 3717–3727.
- [15] P. Heffeter, B. Atil, K. Kryeziu, D. Groza, G. Koellensperger, W. Koerner, U. Jungwirth, T. Mohr, B.K. Keppler, W. Berger, *Eur. J. Cancer* 49 (2013) 3366–3375.
- [16] W.H. Ang, P.J. Dyson, *Eur. J. Inorg. Chem.* (2006) 4003–4018.
- [17] I. Kostova, *Curr. Med. Chem.* 13 (2006) 1085–1107.
- [18] A. Casini, G. Mastrobuoni, M. Terenghi, C. Gabbiani, E. Monzani, G. Moneti, L. Casella, L. Messori, *J. Biol. Inorg. Chem.* 12 (2007) 1107–1117.
- [19] A. Casini, C. Temperini, C. Gabbiani, C.T. Supuran, L. Messori, *ChemMedChem* 5 (2010) 1989–1994.
- [20] M.I. Webb, C.J. Walsby, *Dalton Trans.* 40 (2011) 1322–1331.
- [21] A. Levina, J.B. Aitken, Y.Y. Gwee, Z.J. Lim, M.M. Liu, A.M. Singharay, P.F. Wong, P.A. Lay, *Chem. Eur. J.* 19 (2013) 3609–3619.
- [22] M. Li, L. Lai, Z. Zhao, T. Chen, *Chem. Asian J.* 11 (2016) 310–320.
- [23] M.I. Webb, C.J. Walsby, *Dalton Trans.* 44 (2015) 17482–17493.
- [24] G.K. Gransbury, P. Kappen, C.J. Glover, J.N. Hughes, A. Levina, P.A. Lay, I.F. Musgrave, H.H. Harris, *Metalomics* (2016), accepted, 20/07/2016, DOI: 2010.1039/c2016mt00145a.
- [25] B.R. Cameron, M.C. Darks, I.R. Baird, R.T. Skerlj, Z.L. Santucci, S.P. Fricker, *Inorg. Chem.* 42 (2003) 4102–4108.
- [26] I. Bratsos, G. Birarda, S. Jedner, E. Zangrando, E. Alessio, *Dalton Trans.* (2007) 4048–4058.
- [27] I. Bratsos, S. Jedner, A. Bergamo, G. Sava, T. Gianferrara, E. Zangrando, E. Alessio, *J. Inorg. Biochem.* 102 (2008) 1120–1133.
- [28] T. Gianferrara, A. Bergamo, I. Bratsos, B. Milani, C. Spagnul, G. Sava, E. Alessio, *J. Med. Chem.* 53 (2010) 4678–4690.

- [29] T. Gianferrara, I. Bratsos, E. Iengo, B. Milani, A. Ostric, C. Spagnul, E. Zangrando, E. Alessio, *Dalton Trans.* (2009) 10742–10756.
- [30] B. Serli, E. Zangrando, T. Gianferrara, C. Scolaro, P.J. Dyson, A. Bergamo, E. Alessio, *Eur. J. Inorg. Chem.* (2005) 3423–3434.
- [31] E. Zangrando, N. Kulisic, F. Ravalico, I. Bratsos, S. Jedner, M. Casanova, E. Alessio, *Inorg. Chim. Acta* 362 (2009) 820–832.
- [32] T.M. Santos, B.J. Goodfellow, J. Madureira, J.P. de Jesus, V. Felix, M.G.B. Drew, *New J. Chem.* 23 (1999) 1015–1025.
- [33] G. Sava, I. Capozzi, K. Clerici, G. Gagliardi, E. Alessio, G. Mestroni, *Clin. Exp. Metastasis* 16 (1998) 371–379.
- [34] G.A. Mestroni, E. Sava, G. (1998) WIPO Pat., WO9800431A9800431.
- [35] J. Marques, T.M. Braga, F.A.A. Paz, T.M. Santos, M.D.S. Lopes, S.S. Braga, *Biometals* 22 (2009) 541–556.
- [36] T. Bora, M.M. Singh, *Trans. Metal Chem.* 3 (1978) 27–31.
- [37] TopSpin, Version 3.0, Bruker Biospin, Rheinstetten, Germany, 2007.
- [38] Spinworks, Version 3.0, University of Manitoba, Winnipeg, 2010.
- [39] Pro-Kineticist, Version 1, Applied Photophysics, Leatherhead, UK, 1996.
- [40] P.A. Lay, A. Levina, *Inorg. Chem.* 35 (1996) 7709–7717.
- [41] G.N. George, I.J. Pickering, M.J. Pushie, K. Nienaber, M.J. Hackett, I. Ascone, B. Hedman, K.O. Hodgson, J.B. Aitken, A. Levina, C. Glover, P.A. Lay, *J. Synchrotron Radiat.* 19 (2012) 875–886.
- [42] A.C. Thompson, D.T. Attwood, E.M. Gullikson, M.R. Howells, J.B. Kortright, A.L. Robinson, J.H. Underwood, K.-J. Kim, J. Kirz, I. Lindau, P. Pianetta, H. Winick, G. P. Williams, J.H. Scofield, *X-ray Data Booklet* (2001).
- [43] G.N. George, I.J. Pickering, *Stanford Synchrotron Research Lightsource, California, USA, 2000.*
- [44] W.H. McMaster, D.G. Kerr, J.H. Mallett, J.H. Hubbell, *Compilation of X-ray Cross Sections* (1969).
- [45] OriginLab, vol. 6.1, OriginLab, Northampton, USA, 2000, pp. Origin®.
- [46] M. Roddy, T. Nelson, D.M. Appledorn, V. Groppi, *Essen BioScience Application Note, Essen BioScience Application Note, 2013.*
- [47] C.-L. Hsu, W.-C. Lee, *Int. J. Epidemiol.* 39 (2010) 1597–1604.
- [48] J. Jamrozik, I. Strandén, L.R. Schaeffer, *J. Dairy Sci.* 87 (2004) 699–705.
- [49] A.A. Korneev, A.N. Krichevets, *Psikholog. Zh.* 32 (2011) 97–110.
- [50] J.F. Lucke, *Ann. Emerg. Med.* 28 (1996) 408–413.
- [51] C. Sheridan, H. Kishimoto, R.K. Fuchs, S. Mehrotra, P. Bhat-Nakshatri, C.H. Turner, R. Goulet, S. Badve, H. Nakshatri, *Breast Cancer Res.* 8 (2006) R59.
- [52] C. Brakebusch, D. Bouvard, F. Stanchi, T. Saki, R. Fassler, *J. Clin. Invest.* 109 (2002) 999–1006.
- [53] J.T. Price, E.W. Thompson, *Targets* 6 (2002) 217–233.
- [54] P. Friedl, K. Wolf, *Nat. Rev. Cancer* 3 (2003) 362–374.
- [55] J.C. Chen, L.M. Chen, S.Y. Liao, K. Zheng, L.N. Ji, *Dalton Trans.* (2007) 3507–3515.
- [56] F. Wang, H.M. Chen, S. Parsons, L.D.H. Oswald, J.E. Davidson, P.J. Sadler, *Chem. Eur. J.* 9 (2003) 5810–5820.
- [57] Y.Y. Gwee, *Investigations of the anti-metastatic properties of NAMI-A and its biotransformations in blood (BSc(Hon) thesis), University of Sydney, 2006.*
- [58] I. Bratsos, A. Bergamo, G. Sava, T. Gianferrara, E. Zangrando, E. Alessio, *J. Inorg. Biochem.* 102 (2008) 606–617.
- [59] P.A. Lay, *Inorg. Chem.* 26 (1987) 2144–2149.
- [60] P.A. Lay, *Coord. Chem. Rev.* 110 (1991) 213–233.
- [61] P.A. Lay, *Comm. Inorg. Chem.* 11 (1991) 235–284.
- [62] *Advanced DMEM, Cat. No.12491023, Thermo Fisher Scientific, 2014.*
- [63] M.I. Webb, B. Wu, T. Jang, R.A. Chard, E.W.Y. Wong, M.Q. Wong, D.T.T. Yapp, C.J. Walsby, *Chem. Eur. J.* 19 (2013) 17031–17042.
- [64] L.A. Liotta, W.G. Stetlerstevenson, P.S. Steeg, *Cancer Invest.* 9 (1991) 543–551.
- [65] A. Bergamo, M. Gerdol, M. Lucafo, C. Pelillo, M. Battaglia, A. Pallavicini, G. Sava, *Metalomics* 7 (2015) 1439–1450.
- [66] L. Brescacin, A. Masi, G. Sava, A. Bergamo, *J. Biol. Inorg. Chem.* 20 (2015) 1163–1173.
- [67] A. Levina, P.A. Lay, *Inorg. Chem. Front.* 1 (2014) 44–48.